Inorganic Chemistry

Article

pubs.acs.org/IC

Structural Rearrangement Through Lanthanide Contraction in Dinuclear Complexes

Amy-Jayne Hutchings, Fatemah Habib, Rebecca J. Holmberg, Ilia Korobkov, and Muralee Murugesu*

University of Ottawa, 10 Marie Curie, Ottawa, Ontario, Canada, K1N 6N5

Supporting Information

ABSTRACT: A new series of lanthanide complexes was synthesized, and the geometry and preliminary magnetic measurements of the complexes were explored. The specific ligand used (*N*′-(2-hydroxy-3-methoxybenzylidene)-benzhydrazide) (H_2hmb) was synthesized using a Schiff-base approach and was employed due to the presence of a coordination pocket that is able to accommodate magnetically selective lanthanide ions. The series can be divided into two groups that are categorized by a drastic structural rearrangement. The first group, Type I, contains six analogous complexes with the formula $[M^{III}_2(Hhmb)_3(NCS)_3]\cdot 2MeOH\cdot py$ (M = Y **1**, Eu **2**, Gd **3**, Tb **4**, Dy **5**, Ho **6**), while the second group, Type II, contains two dinuclear complexes with formula $[M^{III}_2(Hhmb)_2(NCS)_4(MeOH)_2]$ (M = Er **7**, and Yb **8**). Single-crystal X-ray analysis revealed that all M^{III} ions in Type I exhibit monocapped distorted square antiprismatic geometries, while those of Type II exhibit distorted dodecahedron geometry. The direct current and alternating current magnetic measurements were carried out on all complexes, with **5**, **7**, and **8** exhibiting slow relaxation of the magnetization under an applied optimum dc field. Furthermore, complex **8** is the first example of a dinuclear Yb-based single-molecule magnet showing field-dependent multiple relaxation processes.

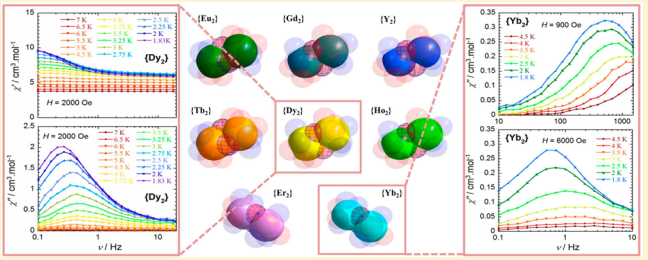

INTRODUCTION

Lanthanide coordination chemistry has consistently been of significant research interest due to its wide range of applications, such as in signal contrast agents,[1] luminescent probes,[2] and magnetic materials.[3] One of the challenges associated with the lanthanide elements is the lack of predictability in terms of their coordination and complex formation. They have a wide range of coordination numbers and geometries that are close in energy due to the decreased ligand field effects experienced by these metal ions. One of the main contributing factors in the versatility and structural changes experienced by the f-block metals is the well-known lanthanide contraction.[4] Across the series La^{III}–Lu^{III} it has been well-documented that the decrease in the ionic radius of the metal ions results in slight rearrangements, leading to differences in coordination number and/or geometry. The changes observed thus far have been relatively subtle,[5,26] with, for example, bidentate coordinating ligands switching to monodentate ligands.[4] However, minor changes can have significant implications on the physical characteristics and observed properties of the lanthanide complexes.

The characteristic magnetic behavior often observed in lanthanide complexes is one example of an interesting inherent property. The heavier lanthanide metals are known to be ideal candidates for molecular magnets because of certain inherent features, such as large numbers of unpaired electrons in shielded 4f orbitals (*S*) coupled with significant spin–orbit interactions (*D*), leading to slow relaxation of the magnetization and single-molecule magnet (SMM) behavior.[6] The recent publication of Pointillart et al. describes the first Yb single-molecule magnet that is redox-activated and has luminescent properties.[7] Dy and Tb SMMs have been dominating the field of SMMs, and this paper demonstrates the feasibility and success of uncommon lanthanide atoms as SMMs.

The properties of lanthanide complexes,[8] their geometry,[9] the precise arrangement, and the orientation of anisotropic axes (where the spin is preferentially aligned)[4,10] are all properties that can be altered due to the presence of donor atoms within the first coordination sphere. Ligand design is a vital tool in the isolation of these complexes, as it plays a role in the stability and encapsulation of metal centers. Lanthanide metal ions are known to have high coordination numbers and large ionic radii; thus, it is necessary to design multidentate ligands with pockets large enough to accommodate lanthanide ions, while still being flexible enough to comply with the steric demands of the molecule. It has been noted that small alterations in ligand design can produce changes in the physical properties of the metal complex.[11] Aromi and co-workers[4d] have recently studied a complete isostructural series of lanthanide dinuclear complexes in which a structural change occurs due to the nitrate group changing from bidentate to monodentate. This change occurs between the Eu and Gd analogues of the series

Received: October 28, 2013

   dx.doi.org/10.1021/ic402682r | *Inorg. Chem.* XXXX, XXX, XXX–XXX

and results in a reduction in coordination number of one metal center from 10- to 9-coordinate. The remaining metal center of the dinuclear complex does not undergo structural changes and remains 10-coordinate for all analogues.

The modulation of the physical characteristics of lanthanide complexes and the corresponding changes in the magnetic properties were investigated in the previously published complex $[Dy_2(hmi)_2(NO_3)_2(MeOH)_2]$, where hmi = 2-hydroxy-3-methoxyphenyl)methylene isonicotino) hydrazine.[12] This dinuclear, 8-coordinate Dy^{III} compound was shown to be arranged as a dinuclear unit, with an energy barrier of U_{eff} = 56 K, or as an assembly of two-dimensional sheets based on the same dinuclear unit, with an energy barrier of U_{eff} = 71 K. The two dysprosium centers were bridged by two phenoxide ligand moieties, leading to dominant ferromagnetic coupling between the metal ions. In comparison, an unsymmetrical dinuclear Dy complex with a comparable bridging motif produced an energy barrier of U_{eff} = 36 K and U_{eff} = 80 K due to two different slow relaxation pathways arising from two crystallographically independent Dy^{III} ions.[13] Therefore, a more thorough fundamental understanding of the characteristics and structural properties of lanthanide metals is needed to fully understand the origins of slow relaxation of the magnetization in these complexes.

In this paper, we attempt to gain more insight into the correlation between a drastic structural rearrangement in a family of lanthanide complexes and the resulting changes in magnetic properties. Herein, we report the syntheses, X-ray structural characterization, and magnetic properties of eight new lanthanide (III) dinuclear complexes, with one group of six analogues with formula $[M^{III}_2(Hhmb)_3(NCS)_3]\cdot 2MeOH\cdot py$ (M = Y **1**, Eu **2**, Gd **3**, Tb **4**, Dy **5**, Ho **6**, Type I) and another group of two analogues with formula $[M^{III}_2(Hhmb)_2(NCS)_4(MeOH)_2]$ (M = Er **7** and Yb **8**, Type II). The ligand H_2hmb (*N*′-(2-hydroxy-3-methoxybenzylidene)benzhydrazide) is shown in Figure 1. This specific ligand was utilized not only

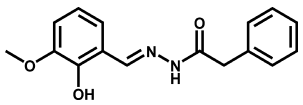

Figure 1. The ligand *N*′-(2-hydroxy-3-methoxybenzylidene)-benzhydrazide (H_2hmb). In all complexes, the deprotonated phenoxy tautomeric form (Hhmb) with a monoanionic charge is coordinated to the metal ions.

because of the presence of a large pocket that would be able to potentially accommodate two lanthanide ions but also because it has five potential chelating sites. While maintaining the Schiff-base ligand and the reaction conditions, we aim to study the effect of the lanthanide contraction on this series of complexes. The decrease of the ionic radius leads to a drastic structural rearrangement for the centrosymmetric dinuclear Er and Yb analogues. In the series presented in this paper, both metal centers of Type I complexes are crystallographically independent and 9-coordinate with distorted monocapped square antiprismatic geometry. As we progress down the series, structural rearrangement occurs between Ho and Er, producing the Type II compounds, which are centrosymmetric with 8-coordinate M^{III} centers and distorted dodecahedron geometry. This series of complexes is believed to be among a rare group of compounds that undergoes such drastic structural rearrangements due to the lanthanide contraction.[14]

EXPERIMENTAL METHODS

Materials. All manipulations were performed under aerobic/ambient conditions. All chemicals were purchased from TCI, Alfa Aesar, and Strem Chemicals and were used without further purification.

Synthesis. *N*′*-(2-hydroxy-3-methoxybenzylidene)benzhydrazide (H_2hmb).* The ligand was synthesized through a condensation reaction, following our previously reported procedure.[15] To a solution of benzhydrazide (2.72 g, 0.02 mol) in methanol (10 mL), a solution of *o*-vanillin (3.04 g, 0.02 mol) in methanol (10 mL) was added. The mixture was stirred for 24 h at room temperature. The resulting white powder was collected through suction filtration and washed with a small amount of methanol. Yield = 85%. Infrared Selected IR data (cm^{-1}): 2060(w), 1655(s), 1605(m), 1572(m), 1534(w), 1466(s), 1405(m), 1375(s), 1347(s), 1248(s), 1164(s), 1088(s), 1076(s), 965(s), 937(s), 774(s), 719(s), 691(s). ^1H NMR (MeOD, 400 MHz): δ 8.56(s, 1H), 7.92(d, 2H), 7.59(t, 1H), 7.48(t, 2H), 7.17(d, 1H), 7.03(d, 1H), 6.85(t, 1H), 3.88(s, 3H).

*$[Y^{III}_2(Hhmb)_3(NCS)_3]\cdot 2MeOH\cdot py$, **1**.* A suspension of $YCl_3\cdot 6H_2O$ (0.076g, 0.25 mmol) in 5 mL of MeOH was added to a solution of H_2hmb (0.067g, 0.25 mmol), NaSCN (0.081g, 1.0 mmol) in 5 mL of MeOH, and pyridine (0.078 mL, 1.0 mmol). The yellow solution was stirred for 5 min and filtered; the filtrate was placed in an ether bath at room temperature. X-ray-quality yellow block crystals were recovered after 7 d. Crystals were collected by vacuum filtration. Yield: 27%. To prevent deterioration, the crystals were kept in contact with the mother liquor and identified crystallographically. Selected IR data (cm^{-1}): 2082(m), 2060(m), 1967(s), 1869(m), 1749(s), 1598(m), 1570(m), 1457(m), 1399(m), 1371(m), 1302(m), 1224(m), 11679(m), 1105(m), 970(m), 898(m),782(m), 747(s), 709(m), 684(m). Anal. Calcd for C 50.31%, H 3.67%, N 10.88%. Found: C 50.48%, H 3.49%, N 10.66%.

*$[Eu^{III}_2(Hhmb)_3(NCS)_3]\cdot 2MeOH\cdot py$, **2**.* This was prepared following the same procedure as for complex **1**. X-ray-quality orange crystals were recovered after 8 d. Crystals were collected by vacuum filtration. Yield: 38%. Selected IR data (cm^{-1}): 2059(s), 1606 (s), 1554(s), 1457(s), 1375(m), 1297(s), 1225(s), 1169(w), 1106(w), 1076(w), 967(m), 898(m), 855(m), 790(w), 740(m), 708(m). Anal. Calcd for C 44.09%, H 3.34%, N 9.49%. Found: C 44.30%, H 3.43%, N 9.66%.

*$[Gd^{III}_2(Hhmb)_3(NCS)_3]\cdot 2MeOH\cdot py$, **3**.* This was prepared following the same procedure as for complex **1**. X-ray-quality orange block crystals were recovered after 4 d. Crystals were collected by vacuum filtration. Yield: 42%. Selected IR data (cm^{-1}): 2073(w), 2055(w), 1602(w), 1569(s), 1553(w), 1454(w), 1401(m), 1371(w), 1299(w), 1222(w), 1168(m), 1103(s), 1075(m), 1026(s), 965(w), 898(w), 855(m), 790(m), 738(w), 709(m). Anal. Calcd for C 44.17%, H 3.43%, N 9.32%. Found: C 43.93%, H 3.39%, N 9.51%.

*$[Tb^{III}_2(Hhmb)_3(NCS)_3]\cdot 2MeOH\cdot py$, **4**.* This was prepared following the same procedure as for complex **1**. X-ray-quality yellow block crystals were recovered after 5 d. Crystals were collected by vacuum filtration. Yield: 31%. Selected IR data (cm^{-1}): 2077(w), 2058(w), 1604(w), 1570(s), 1554(w), 1455(w), 1401(s), 1371(s), 1299(w), 1222(w), 1167(s), 1105(s), 1076(w), 1025(s), 964(m), 898(w), 855(m), 791(m), 738(m). Anal. Calcd for C 43.56%, H 3.42%, N 9.29%. Found: C 43.66%, H 3.58%, N 9.42%.

*$[Dy^{III}_2(Hhmb)_3(NCS)_3]\cdot 2MeOH\cdot py$, **5**.* This was prepared following the same procedure as for complex **1**. X-ray-quality yellow block crystals were recovered after 3 d. Crystals were collected by vacuum filtration. Yield: 32%. Selected IR data (cm^{-1}): 2080(w), 2064(w), 1604(m), 1572(s), 1298(m), 1219(m), 1068(s), 890(s), 731(m). Anal. Calcd for C 45.73%, H 3.41%, N 9.88%. Found: C 45.52%, H 3.44%, N 9.66%.

*$[Ho^{III}_2(Hhmb)_3(NCS)_3]\cdot 2MeOH\cdot py$, **6**.* This was prepared following the same procedure as for complex **1**. X-ray-quality pink block crystals were recovered after 5 d. Crystals were collected by vacuum filtration. Yield: 36%. Selected IR data (cm^{-1}): 2080(w), 2061(w), 1605(w), 1571(s), 1552(m), 1458(w), 1401(m), 1372(m), 1300(w), 1224(w), 1169(s), 1106(s), 1074(m), 1025(s), 964(m), 899(w), 856(m),

dx.doi.org/10.1021/ic402682r | *Inorg. Chem.* XXXX, XXX, XXX–XXX

788(s), 739(m), 710(m). Anal. Calcd for C 44.88%, H 3.10%, N 9.85%. Found: C 44.65%, H 3.33%, N 9.58%.

$[Er^{III}_2(Hhmb)_2(NCS)_4(MeOH)_2]$, **7**. This was prepared following the same procedure as for complex **1**. X-ray-quality clear crystals were recovered after 4 d. Crystals were collected by vacuum filtration. Yield: 30%. Selected IR data (cm^{-1}): 2095(s), 2059(s), 1618(s), 1551(s), 1457(m), 1396(m), 1314(m), 1221(s), 1080(m), 1064(w), 965(m), 900(m), 848(m), 785(m), 749(w), 736(m), 680(m), 642(w). Anal. Calcd for C 37.06%, H 3.27%, N 9.10%. Found: C 37.26%, H 3.12%, N 9.30%.

$[Yb^{III}_2(Hhmb)_2(NCS)_4(MeOH)_2]$, **8**. This was prepared following the same procedure as for complex **1**. X-ray-quality clear crystals were recovered after 4 d. Crystals were collected by vacuum filtration. Yield: 25%. Selected IR data: 2093(s), 2061(s), 1618(s), 1553(m), 1456(s), 1396(m), 1312(m), 1224(s), 1080(m), 967(m), 897(m), 845(w), 785(m), 747(w), 739(m), 681(w), 645(w). Anal. Calcd for C 36.66%, H 3.40%, N 9.00%. Found: C 36.40%, H 3.29%, N 9.21%.

IR, Elemental Analysis, X-ray Powder Diffraction, and NMR Measurements. Infrared spectra were recorded in the solid state on a Varian 640 FT-IR spectrometer in the 400−4000 cm^{-1} range. X-ray powder diffraction experiments were performed using a RIGAKU Ultima IV, equipped with a Cu Kα radiation source (λ = 1.541836 Å) and a graphite monochromator. Scanning of the 2θ range was performed from 5 to 40°, depending on the particular sample, and compared with calculated patterns from single-crystal X-ray data. To assign the peaks corresponding to particular crystalline phases, PDXL software equipped with the RIGAKU apparatus was used with the ICDD database. Elemental analysis was performed at Canadian Microanalytical Service Ltd. NMR analyses were conducted on a Bruker Avance 400 spectrometer equipped with an automatic sample holder and a 5 mm autotuning broadband probe with Z gradient.

X-ray Crystallography. For all compounds, a single crystal was mounted on a glass fiber. A Bruker APEX-II CCD device was used to collect unit cell and intensity data using graphite Mo Kα radiation (λ = 0.71073). The data reduction included a correction for Lorentz and polarization effects, with an applied multiscan absorption correction (SADABS).

The crystal structures were solved and refined using the SHELXTL program suite.[16] Direct methods yielded all non-hydrogen atoms, which were refined with anisotropic thermal parameters. All hydrogen atom positions were calculated geometrically and were riding on their respective atoms.

Magnetic Measurements. Magnetic measurements were obtained using a Quantum SQUID magnetometer MPMS-XL7 operating between 1.8 and 300 K for direct current (dc) applied fields ranging from −7 to 7 T. Dc analyses were performed on polycrystalline samples of 19.2, 16.8, 12.1, 9.1, 15.8, 8.4, and 16.3 mg of complexes **2**−**8**, respectively, wrapped in a polyethylene membrane. Alternating current (ac) susceptibility measurements were carried out under an oscillating ac field of 3 Oe and ac frequencies ranging from 0.1 to 1500 Hz. The magnetization data were collected at 100 K to check for ferromagnetic impurities that were absent in all samples. Diamagnetic corrections were applied for the sample holder and the diamagnetism from the sample (estimated with Pascal constants).

RESULTS AND DISCUSSION

The Schiff-base ligand H_2hmb was synthesized through a condensation reaction of *o*-vanillin and benzhydrazide. This ligand provides two multidentate pockets that can easily accommodate lanthanide metal centers, as displayed in Figure 2. Schiff-base reactions are relatively simple synthetically and can be high-yielding. The *o*-vanillin moiety has previously been used in the synthesis of many lanthanide-based complexes[17] with novel magnetic properties and is a perfect candidate for Schiff-base reactions. In addition, the phenoxy atoms of the *o*-vanillin starting material can be deprotonated to act as a bridge between metal centers, creating a super-exchange pathway. This ligand system is particularly enticing because it easily allows for

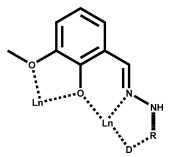

Figure 2. Potential coordination modes of H_2hmb ligand, demonstrating the encapsulation of two metal centers and the presence of an R group, which could contain further donor atoms (D).

the modification of the R group to create a series of slightly varied ligand systems to study the fundamental magnetic and structural properties of lanthanide complexes. The modification of the R group can also lead to a potential increase in the number of metal centers within the lanthanide cluster, as demonstrated in Figure 2.[18]

The stoichiometric reaction of H_2hmb and $LnCl_3{\cdot}xH_2O$ in the presence of pyridine (4 equiv) in MeOH resulted in the crystallization of eight dinuclear complexes $[Ln^{III}_2(Hhmb)_3(NCS)_3]{\cdot}2MeOH{\cdot}py$ (Ln = Y^{III} **1**, Eu^{III} **2**, Gd^{III} **3**, Tb^{III} **4**, Dy^{III} **5**, Ho^{III} **6**, Type I) and $[Ln^{III}_2(Hhmb)_2(NCS)_4(MeOH)_2]$ (Ln = Er^{III} **7**, and Yb^{III} **8**, Type II). The presence of the pyridine base was necessary to deprotonate the ligand, allowing the phenoxy group to partake in coordination and bridging between metal ions. Complexes of Type I were also isolated with variations in solvents (EtOH and MeOH/MeCN), as the solvent molecules do not coordinate to metal ions in these dinuclear complexes. The solvents are, however, found to crystallize within the unit cell. The highest-yielding reaction was found when using MeOH. X-ray powder diffraction (XRPD) experiments were performed to ascertain the bulk phase purity of the crystalline materials. A comparative study was performed between calculated patterns obtained through single-crystal X-ray data and XRPD patterns taken of bulk crystalline samples containing the following metals: Y(III), Eu(III), Gd(III), Dy(III), Ho(III), Er(III), and Yb(III). These comparisons exhibited a definite matching of peaks (Supporting Information, Figures S1−S7); thus, we can confirm that the bulk phase purity is consistent with the single-crystal data obtained. Elemental analysis was also employed to confirm bulk sample purity.

Single-crystal X-ray studies reveal that all six compounds in Type I are isostructural and crystallize in the triclinic $P\bar{1}$ space group (Table 1). As an example, the structure of the dysprosium analogue, complex **5**, will be described in detail and represents all Type I compounds (Figure 3, top). The dinuclear complex is composed of two 9-coordinate Dy^{III} ions bridged by three μ-phenoxides of the Hhmb ligands (O1, O4, and O7), with bond angles of Dy1−O1−Dy2, 100.8°; Dy1−O4−Dy2, 96.1°; and Dy1−O7−Dy2, 101.1°, as displayed in Figure 4.

The two Dy centers of complex **5** are separated by an intramolecular distance of 3.56 Å. Dy1 is bound to three ligands (O1, O2, O4, O6, O7, O9, N3, and N6) and one isothiocyanate anion (N7), whereas Dy2 is surrounded by three ligands (O1, O3, O4, O5, O7, O8, N1) and two isothiocyanate molecules (N8, N9). Both metal centers exhibit distorted monocapped square antiprism geometry, as displayed in Figure 4, bottom. The Dy1 ion is capped by O9, with the top square composed of the O1, O2, O6, and the N5 atoms, while the bottom square is composed of the O4, O7, N3, and N7 atoms. The Dy2 ion is capped by N1, with the top square composed of the O1, O3, N8, and N9 atoms, while the bottom square is composed of the

dx.doi.org/10.1021/ic402682r | Inorg. Chem. XXXX, XXX, XXX−XXX

Table 1. Crystallographic Data of the Dinuclear Complexes 1−8

	1	2	3	4
formula	$C_{51.25}H_{44.50}Y_2N_{9.50}O_{9.75}S_3$	$C_{48.75}H_{44}Eu_2N_9O_{10.75}S_3$	$C_{49.75}H_{46}Gd_2N_9O_{10.75}S_3$	$C_{49.25}H_{46}Tb_2N_9O_{11.25}S_3$
fw	1223.46	1328.03	1352.64	1357.97
T (K)	200(2)	200(2)	200(2)	200(2)
crystal system	triclinic	triclinic	triclinic	triclinic
space group	$P\bar{1}$	$P\bar{1}$	$P\bar{1}$	$P\bar{1}$
a/Å	11.5128(2)	11.6015(3)	11.7591(3)	11.7308(5)
b/Å	14.9324(3)	15.0634(3)	14.9848(3)	15.0179(6)
c/Å	18.7898	19.1116(4)	19.0708(4)	19.0123(7)
α/deg	106.9750(10)	107.9010(10)	108.1350(10)	108.212(2)
β/deg	100.0730(10)	99.7990(10)	99.8990(10)	100.0090(10)
γ/deg	105.8750(10)	105.9500(10)	104.6680(10)	105.4310(10)
vol/Å^3	2855.44(10)	2935.11(11)	2952.07	2943.72
Z	2	2	2	2
DC/Mg m^{-3}	1.423	1.503	1.522	1.532
μ/mm^{-1}	2.193	2.283	2.393	2.550
reflns collected	37814	17568	42586	43144
GOF	1.047	1.033	1.018	1.047
$R1$, $wR2$ ($>2\sigma(I)$)[a]	0.0450, 0.1330	0.0330, 0.0935	0.0341, 0.0970	0.0429, 0.1158
$R1$, $wR2$ (all data)	0.0642, 0.1436	0.0425, 0.0998	0.0427, 0.1057	0.0530, 0.1232
	5	**6**	**7**	**8**
formula	$C_{54}H_{48}Dy_2N_{10}O_{10}S_3$	$C_{50.50}H_{41.50}Ho_2N_{9.50}O_9S_3$	$C_{19}H_{20}ErN_4O_5S_2$	$C_{19}H_{20}YbN_4O_5S_2$
fw	1418.20	1351.47	615.77	622.56
T (K)	200(2)	200(2)	200(2)	200(2)
crystal system	triclinic	triclinic	triclinic	triclinic
space group	$P\bar{1}$	$P\bar{1}$	$P\bar{1}$	$P\bar{1}$
a/Å	11.6009(3)	11.7069(2)	9.7922(7)	9.7648(2)
b/Å	14.9562(3)	14.9767(3)	10.3359(7)	10.3240(2)
c/Å	18.8967(6)	18.9807(4)	11.9250(8)	11.8846(2)
α/deg	107.7620(10)	108.3730(10)	97.488(3)	97.2840(10)
β/deg	100.1620(10)	99.9320(10)	94.448(3)	94.6080(10)
γ/deg	105.3460(10)	105.4420(10)	103.038(3)	102.8900(10)
vol/Å^3	2890.60(13)	2922.38	1158.63(14)	1151.16(4)
Z	2	2	2	2
DC/Mg m^{-3}	1.629	1.536	1.765	1.796
μ/mm^{-1}	2.738	2.853	3.838	4.280
reflns collected	30 594	25 781	7099	11 608
GOF	1.080	1.062	1.026	1.032
$R1$, $wR2$ ($>2\sigma(I)$)[a]	0.0645, 0.1094	0.0332, 0.0896	0.0244, 0.0567	0.0143, 0.0374
$R1$, $wR2$ (all data)	0.1103, 0.1304	0.0462, 0.0988	0.0291, 0.0607	0.0151,0.0379

[a] $R = R_1 = \sum||F_o| - |F_c||/\sum|F_o|$; $wR_2 = \{\sum[w(F_o^2 - F_c^2)^2]/\sum[w(F_o^2)^2]\}^{1/2}$; $w = 1/[\sigma^2(F_o^2) + (ap)^2 + bp]$, where $p = [\max(F_o^2,0) + 2Fc^2]/3$.

O4, O5, O7, and O8 atoms. Selected bond distances (Å) and angles (deg) of the Dy analogue **5** are listed in Table 2.

Comparable phenoxy bridging motifs found in dinuclear dysprosium complexes reported by Lin et al.[19] and Patroniak et al.[20] produced similarly separated metal centers, with an intramolecular Dy···Dy distance of 3.49 Å and 3.59 Å, respectively. The metal ions of the dinuclear complexes **1**−**8** are located in the hypothesized pocket of the ligand, as shown in Figure 2, and coordinate to the methoxy, phenoxy, imine, and ketone elements of the ligand. This permits the isothiocyanate molecules to asymmetrically complete the coordination sphere of each Dy center. The packing arrangement along the a axis of complex **5** is shown in Figure 5 (top), and packing along the b and c axes can be found in the Supporting Information (Figure S8). Along the a axis, it can be seen that the dinuclear complex is well-isolated, with the shortest intermolecular Dy1···Dy1 distance being 8.56 Å and the smallest Dy2···Dy2 distance being 13.23 Å, compared to the intramolecular distance of Dy1···Dy2 of 3.56 Å. The molecules are aligned in an antiparallel fashion and pack in an ABA arrangement.

The structure of the erbium analogue, complex **7**, will be described in detail and represents the Type II compounds (Figure 3, bottom). The dinuclear complex is composed of two 8-coordinate Er^{III} ions bridged by two μ-phenoxides of the Hhmb ligands (O1), with a bond angle of Er1−O1−Er1 106.89°, as displayed in Figure 6. Unlike Type I, the Type II compounds are centrosymmetric with an intramolecular Er1··· Er1a distance of 3.39 Å.

Each Er^{III} ion is bound to two ligands (O1, O1a, O2, O3, and N1), two isothiocyanate anions (N3 and N4), and one methanol coordinating solvent molecule (O4). The Er centers adopt a distorted dodecahedron geometry, as displayed in Figure 6. The pentagonal plane is composed of the ligand atoms O1, O1a, O2, O3, and N1, while the interpenetrating triangle is composed of O4, N3, and N4. Selected bond distances (Å) and angles (deg) of the Er analogue **7** are listed in Table 2.

dx.doi.org/10.1021/ic402682r | Inorg. Chem. XXXX, XXX, XXX−XXX

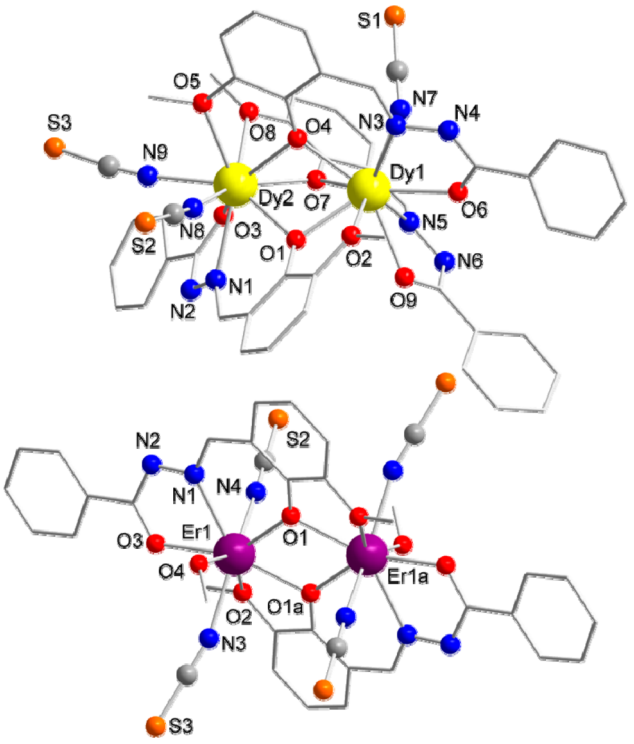

Figure 3. (top) Molecular dinuclear structure of $[Dy^{III}_2(Hhmb)_3(NCS)_3]$, complex **5**. (bottom) Molecular dinuclear structure of $[Er^{III}_2(Hhmb)_2(NCS)_4(MeOH)_2]$, complex **7**. Color code: yellow (Dy), purple (Er), red (O), blue (N), gray (C), orange (S). Hydrogen atoms and solvent molecules have been removed for clarity.

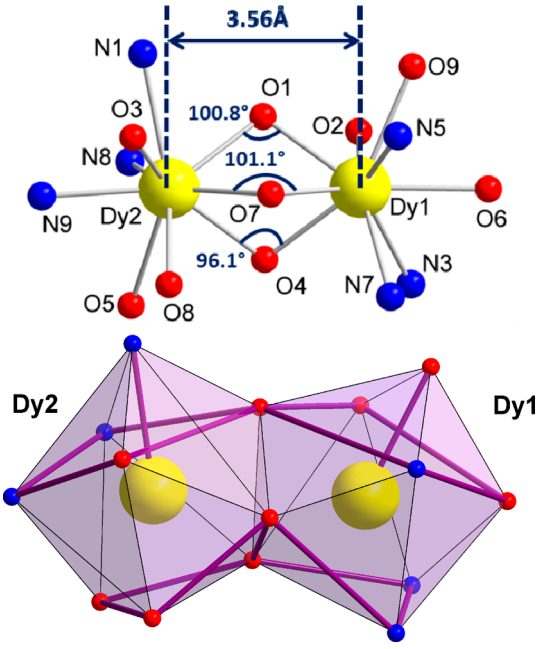

Figure 4. (top) Dinuclear core structure of complex **5**, with selected bridging angles and intermetallic distance. (bottom) Coordination polyhedra of the metal ions in complex **5** displaying the 9-coordinate, monocapped distorted square antiprismatic geometry of both metal centers. Color code: yellow (Dy), red (O), and blue (N); the coordination polyhedra are shown in purple.

The coordination mode of the isothiocyanate groups can be identified through IR spectroscopy; a sharp peak at 2100 cm^{-1} indicates a terminal coordination through the N atom.[21] Each of the three isothiocyanate groups has a slightly different arrangement within complex **5** and, by extension, all of the Type I compounds; S1 has a Dy1−N7−S1 angle of 157.54° and a Dy1···S1 distance of 5.18 Å; S2 has a Dy2−N8−S2 angle of 172.99° and a Dy2···S2 distance of 5.18 Å; and S3 has a Dy2−N9−S3 angle of 167.87° and a Dy2···S3 distance of 5.14 Å. In addition, the isothiocyanate ligands within complex **7** (Type II) have varying arrangements; S2 has an Er1−N4−S2 angle of 178.02°, and S3 has an Er1−N3−S3 angle of 165.76°. Other dysprosium complexes exhibiting terminal isothiocyanate groups have been previously reported;[22] however, we believe this is the only dysprosium complex that is triply bridged by μ-phenoxide with terminal isothiocyanates. The packing arrangement along the *a* axis of complex **7** is shown in Figure 5, bottom, while the packing along the *b* and *c* axes can be found in the Supporting Information (Figure S9). Along the *a* axis, it can be seen that the dinuclear complex is well-isolated, with the smallest intermolecular Er1···Er1 distance being 10.93 Å and the smallest intramolecular Er1···Er1 distance being 3.39 Å. The well-isolated molecules are aligned in a parallel fashion along all crystallographic axes.

Upon examination of the space-filling diagram of complex **5**, it is noted that the sulfur terminal atoms (S1, S2, and S3) for Type I compounds are available for bonding and systematic modification (Figure 7). It is well-known that sulfur atoms have a high affinity to a number of different soft metals;[23] therefore, it is theoretically possible to attach these complexes to different metal substrates such as Au surfaces.[24] Sterically, it would be possible for both the S2 and S3 atoms of complex **5** to attach to this substrate simultaneously. The bulky phenyl group sterically interrupts the possibility of S1 and S2 attaching at the same time, while the methoxy group of the Hhmb ligand blocks S1 and S3 from anchoring simultaneously on a surface.

When we examine the space-filling diagram of the Er analogue **7** (Figure 8), it is evident that attaching to a surface is much more favorable using two of the four S atoms, above or below the plane of the molecule that is occupied by the Hhmb ligands. The alignment of the isothiocyanate groups allows the entire molecule to "sit" on a surface where the surface−sulfur interactions would keep it upright. The structural rearrangement and the difference in coordination polyhedra between the two groups of complexes are directly attributed to the lanthanide contraction. Because of the fact that the reaction conditions were maintained throughout the entire series, the decreasing radii of the late lanthanide metals had caused the dinuclear structure to adopt a more energetically and sterically favorable conformation. All complexes can be viewed in Figure 9, arranged in increasing order of ionic radii to demonstrate how the coordination environment changes for the two smallest ionic radii (Er^{III} = 0.088 nm; Yb^{III} = 0.086 nm).[25]

Following the calculations performed by Raymond and coworkers[26] to determine if a series of compounds can be considered analogous, the shape measure approach was utilized, where the dihedral angles of coordination polyhedra were compared to a reference compound based upon the following equation:

$$AM = \min\left[\sqrt{\frac{1}{m}\sum_{i=1}^{m}(\delta_i - \theta_i)^2}\right] \quad \text{(Eq. 1)}$$

where AM = analogous measurement, δ_i = dihedral angle of the coordination polyhedron along the edge of interest, and θ_i =

dx.doi.org/10.1021/ic402682r | Inorg. Chem. XXXX, XXX, XXX−XXX

Table 2. Selected Bond Distances (Å) and Angles (deg) for Complexes 5 and 7

bond distances (Å)					
complex 5				complex 7	
Dy1−O1	2.310(3)	Dy2−O1	2.295(3)	Er1−O1	2.261(2)
Dy1−O7	2.322(3)	Dy2−O7	2.290(3)	Er1−O1a	2.327(2)
Dy1−N8	2.399(4)	Dy2−O4	2.357(3)	Er1−O2	2.456(2)
Dy1−O9	2.431(4)	Dy2−O6	2.393(3)	Er1−O3	2.286(2)
Dy1−N7	2.422(5)	Dy2−O3	2.439(3)	Er1−O4	2.367(2)
Dy1−O4	2.435(3)	Dy2−N9	2.488(4)	Er1−N1	2.484(3)
Dy1−N5	2.554(4)	Dy2−N3	2.544(4)	Er1−N3	2.368(3)
Dy1−O2	2.566(3)	Dy2−N1	2.546(4)	Er1−N4	2.376(3)
Dy1−O5	2.576(4)	Dy2−O8	2.621(3)	S2−C17	1.635(3)
Dy1−Dy2	3.556(3)	S1−C46	1.639(6)	S3−C16	1.630(4)
N9−C48	1.157(5)	S2−C47	1.622(6)	C16−N3	1.145(4)
N7−C46	1.160(7)	S3−C48	1.644(5)	C17−N4	1.151(4)
bond angles (deg)					
complex 5				complex 7	
Dy1−O1−Dy2	100.86	Dy1−N7−S1	157.54	Er1−N3−S3	165.76
Dy1−O4−Dy2	96.13	Dy2−N8−S2	172.99	Er1−N4−S2	178.02
Dy1−O7−Dy2	101.08	Dy2−N9−S3	167.87	Er1−O2−C2	114.55

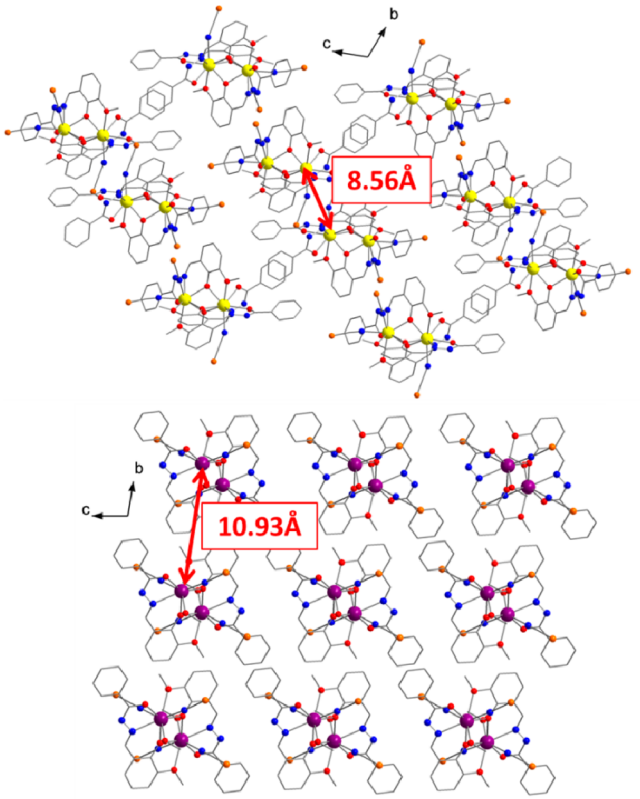

Figure 5. (top) Packing arrangement of complex 5 along the crystallographic *a* axis. Color code: yellow (Dy), red (O), blue (N), orange (S), and gray (C). (bottom) Packing arrangement of complex 7 along the crystallographic *a* axis. Color code: purple (Er), red (O), blue (N), orange (S), and gray (C). Hydrogen atoms and solvents of crystallization have been omitted for clarity.

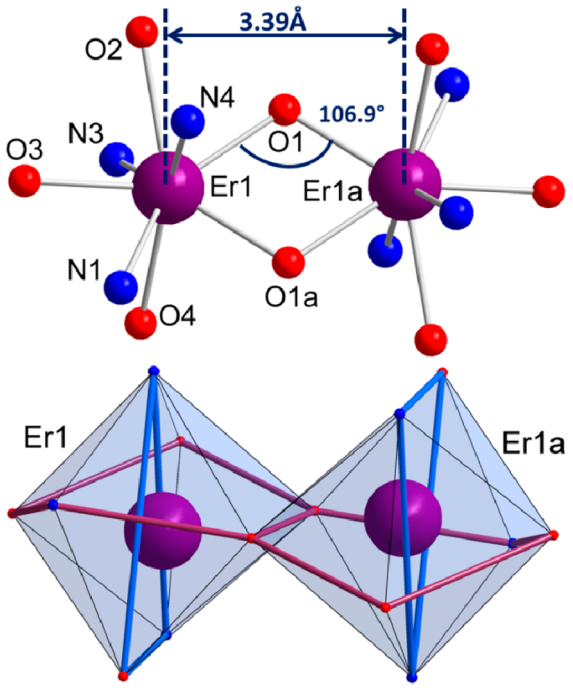

Figure 6. (top) Dinuclear core structure of complex 7, with selected bridging angles and intermetallic distance indicated. (bottom) Coordination polyhedra of the metal ions in complex 7 displaying the 8-coordinate, distorted dodecahedron geometry. Color code: purple (Er), red (O), and blue (N).

dihedral angle from the reference polyhedron, and m = number of dihedral angles. When compound **5**, the $\{Dy_2\}$ analogue, was taken as the reference molecule, it was found that the dihedral angles of the Y (**1**), Gd (**3**) and Ho (**6**) vary only by 0−1.5°. The AM of complexes **1**, **3**, and **6** was calculated to be 0.520, 0.760, and 0.619, respectively, against the reference polyhedron of complex **5** (Table 3). When the AM of complexes **2** and **4** (the $\{Eu_2\}$ and $\{Tb_2\}$ compounds, respectively) was performed with complex **5** as the reference polyhedron, a drastic change in dihedral angles was observed (up to a 70° difference), with an AM of approximately 10. However, an AM of complex **2** $\{Eu_2\}$ was calculated to be 0.717 when complex **4** ($\{Tb_2\}$ analogue) was used as the reference polyhedron (Supporting Information, Table S1). Upon closer inspection, it was discovered that complexes **2** and **4** take a slightly different orientation than that of complexes **1**, **3**, **5**, and **6** but maintain the 9-coordinate monocapped distorted square antiprismatic geometry. This

dx.doi.org/10.1021/ic402682r | Inorg. Chem. XXXX, XXX, XXX−XXX

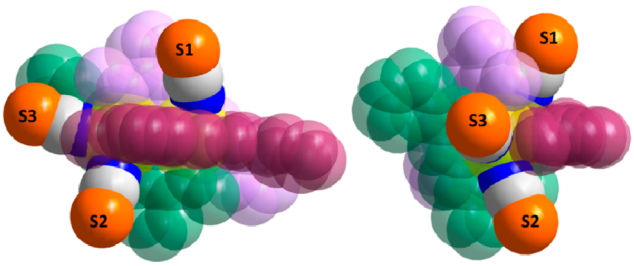

Figure 7. Space-filling diagram of complex **5** to demonstrate the steric availability of the three terminal sulfur atoms. Color code: yellow (Dy), blue (N), gray (C), orange (S). The three Hhmb ligands are shown in light purple, maroon, and green.

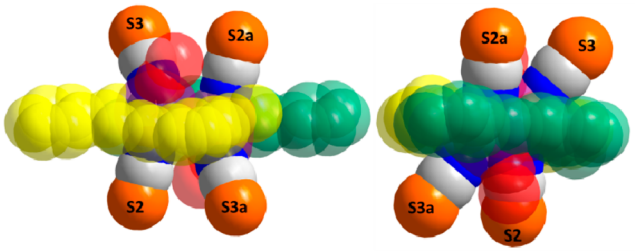

Figure 8. Space-filling diagram of complex **7** to demonstrate the steric availability of the four terminal sulfur atoms. Color code: purple (Er), blue (N), gray (C), orange (S), red (methanol ligands). The two Hhmb ligands are shown in yellow and green.

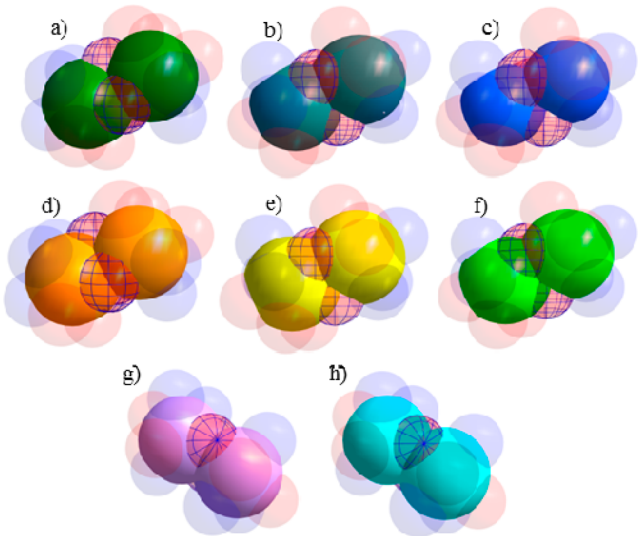

Figure 9. Schematic representation of the different analogues of complexes **1**–**8** arranged in order of decreasing ionic radii (nm). (a) Eu^{III} (0.095). (b) Gd^{III} (0.094). (c) Y^{III} (0.093). (d) Tb^{III} (0.092). (e) Dy^{III} (0.091). (f) Ho^{III} (0.089). (g) Er^{III} (0.088). (h) Yb^{III} (0.086). Complexes (a–f) are orientated along the crystallographic *a* axis. Complexes (g) and (h) are displayed along the crystallographic *b* axis. Coordinating molecules that form the coordination polyhedra are faded, and bridging μ-phenoxide oxygen atoms are highlighted.

different orientation can also be observed upon close examination of Figure 9. However, a mixture of enantiomers or different conformations was not found in the packing arrangements of individual complexes. The origins of these variations are not clear, but they can be attributed to different factors such as geometrical constraints of the multidentate ligand, ligand field effects, and/or the change in ionic radii of the lanthanide centers. In addition, the AM of complex **8** was calculated to be 0.767 when complex **7** was used as a reference (Supporting Information, Table S2). This leads us to consider the possibility that rather than accepting the previously assigned grouping of the series into two types, it is perhaps more accurate to classify the complexes as Type Ia (complexes **1**, **3**, **5**, and **6**), Type Ib (complexes **2** and **4**), and Type II (complexes **7** and **8**).

The change in O–O and Ln–O bond distances of complexes **2**–**8** against the number of 4f electrons is presented in Figure 10. The change in O–O edge length was examined due to the constraint of the multidentate ligand upon the coordination polyhedra of the molecule. In complexes **2**–**6**, there is a total of 10 O–O edges within the coordination sphere of the metal centers, while in **7** and **8** there are a total of five. The O–O distances used in Figure 10 were obtained by averaging all O–O edges in the coordination polyhedra of both metal centers. It is noteworthy that these O–O distances also provide evidence toward three groups of compounds within the lanthanide series (Figure 10, top). A quadratic decay is evident on the graph where the Type Ia compounds (Gd, Dy, and Ho) lie below the fit line, while the Type Ib (Eu and Tb) and Type II (Er and Yb) analogues lie above the fit line. Moreover, there is a decrease in the O–O edge lengths of 3.43%, 3.07%, and 2.74% for Types Ia, Ib, and II, respectively. In addition, the Ln–O distances were plotted (Figure 10, bottom) as evidence for the lanthanide contraction. The O–O distance was expected to decrease in a nonlinear fashion due to the physical constraints of the ligand environment, meaning that not all bonds are able to decrease uniformly.[27] The decrease in Ln–O bond lengths, however, follows a linear decrease; it is expected that as the ionic radius decreases, the Ln–O bonds will contract uniformly within the coordination sphere. The Ln–O bonds decreased by 3.64%, 3.07%, and 2.20% for Types Ia, Ib, and II, respectively. These values are slightly lower than the expected 5–7% decrease as described by Raymond and co-workers.[27]

Magnetic Properties. Complex **1**, the $\{Y_2\}$ analogue, is diamagnetic and hence will not be discussed in this section. The dc magnetic susceptibility measurements for complexes **2**–**8** were carried out in an applied magnetic field of 1000 Oe in the range of 1.8 to 300 K (Figure 11). The room-temperature χT values of 2.37 (**2**), 15.21 (**3**), 23.05 (**4**), 27.65 (**5**), 27.79 (**6**), 24.00 (**7**), and 4.87 (**8**) cm^3 K mol^{-1} are in reasonable agreement with the expected values (**3**: 15.76; **4**: 23.63; **5**: 28.34; **6**: 28.16; **7**: 22.96; **8**: 5.14 cm^3 K mol^{-1}) for two uncoupled lanthanide ions: Gd^{III} ($^8S_{7/2}$, $S = 7/2$; $L = 0$, $g = 2$), Tb^{III} ($^7F_6$, $S = 5/2$, $L = 3$, $g = 3/2$), Dy^{III} ($^6H_{15/2}$, $S = 5/2$, $L = 5$, $g = 4/3$), Ho^{III} ($^5I_8$, $S = 2$, $L = 6$, $g = 5/4$,), Er^{III} ($^4I_{15/2}$, $S = 3/2$, $L = 6$, $g = 6/5$), Yb^{III} ($^2F_{7/2}$, $S = 1/2$, $L = 3$, $g = 8/7$). The observed χT product at room temperature for the Eu^{III} analogue, **2**, is attributed to the presence of thermally populated excited states. At low temperature (1.8 K) the nonmagnetic ground state is observed with $\chi T = 0.02$ cm^3 K mol^{-1}. For **5**, the χT value remains relatively constant before decreasing below 50 K. Below 5 K, it begins to increase again, indicating ferromagnetic interactions at very low temperature. For **3**, **4**, and **6**–**8**, the decrease in the χT value continues below 5 K, indicating low-lying excited states and/or the presence of magnetic anisotropy with no ferromagnetic interactions. The difference in magnetic behavior of different analogues has been previously observed and explained by Ishikawa et al.[27] using ligand-field (LF) parameter calculations on each lanthanide site in homo- and hetero-dinuclear systems. Because of the

dx.doi.org/10.1021/ic402682r | Inorg. Chem. XXXX, XXX, XXX–XXX

Table 3. Dihedral Angles along the Edges of the Coordination Polyhedra Used to Determine the Analogous Measurement (AM) of Complexes 1, 3, and 6 When Using Complex 5 as the Reference Polyhedron[a]

dihedral angle	complex **1** {Y}	complex **3**{Gd}	complex **5** {Dy}	complex **6** {Ho}
O8−O5−O4/\O5−N9−O8	61.298(77)	60.792(110)	61.338(218)	61.653(174)
O8−O5−O4/\N8−O5−O4	70.045(90)	69.403(127)	69.344(237)	68.528(177)
O4−O5−O8/\O4−O7−O8	29.852(73)	29.838(94)	30.316(209)	30.297(155)
O5−N9−08/\N9−O5−N8	58.047(107)	56.987(134)	57.01(25)	56.495(193)
O5−N9−O8/\O8−N9−O3	40.039(91)	41.090(126)	40.374(212)	40.667(177)
O3−O8−N9/\O8−O3−O7	57.739(88)	57.798(137)	57.936(235)	58.109(164)
O3−O8−N9/\N1−O3−N9	52.922(90)	52.451(135)	52.929(222)	51.549(177)
O3−O8−O7/\N1−O3−O7	49.887(89)	48.991(132)	49.600(228)	50.127(175)
O3−O8−O7/\O8−O4−O7	58.779(74)	59.265(101)	58.647(210)	58.254(138)
N9−O3−N1/\N8−N1−N9	42.52(10)	43.658(128)	42.623(232)	44.296(182)
N9−O3−N1/\O3−N1−O7	76.317(73)	75.034(100)	75.863(184)	75.554(146)
O3−N1−O7/\O1−O7−N1	8.647(75)	8.464(108)	8.368(215)	7.645(171)
N1−O7−O1/\N1−O1−N8	72.115(84)	71.460(102)	71.966(221)	71.996(176)
O7−O4−O1/\O4−O7−O8	49.883(73)	50.448(91)	49.726(192)	49.974(128)
O7−O4−O1/\N7−O7−O4	53.435(78)	52.140(103)	52.835(212)	52.885(173)
O7−O4−O1/\O1−O7−N5	60.513(81)	59.988(105)	60.646(204)	59.826(159)
O1−O7−O4/\N1−O7−O1	58.058(77)	57.607(94)	57.79(21)	57.823(164)
O7−O4−O1/\O4−O1−N8	57.874(84)	56.862(107)	57.622(220)	57.388(166)
O7−O4−O1/\O4−O1−O2	47.229(67)	48.113(97)	47.194(200)	47.708(139)
O1−O4−N8/\O4−O1−O2	74.897(88)	75.025(102)	75.184(218)	74.905(146)
O1−O4−N8/\O4−O5−N8	30.329(100)	31.954(122)	31.018(242)	31.828(168)
O4−O5−N8/\N8−O5−N9	63.251(94)	62.796(113)	63.657(230)	63.652(156)
N8−O5−N9/\N8−N9−N1	44.491(94)	46.690(113)	45.288(251)	45.435(170)
N8−N9−N1/\N9−O3−N1	42.520(97)	43.658(127)	42.623(238)	44.296(187)
N8−N9−N1/\N8−N1−O1	58.596(85)	57.753(117)	58.457(214)	58.142(191)
N1−O1−N8/\N1−O1−O7	72.115(77)	71.460(124)	71.966(226)	71.996(184)
N1−O1−N8/\O4−O1−N8	45.448(91)	45.990(123)	45.902(237)	46.015(175)
O4−O7−N7/\O4−O7−O8	76.682(80)	77.412(102)	77.439(208)	77.141(153)
O4−O7−N7/\N3−N7−O4	39.701(84)	40.166(100)	39.655(237)	39.836(179)
O4−O7−N7/\N7−O7−N5	47.639(78)	48.317(107)	48.432(211)	48.336(169)
N3−O4−N7/\O6−N3−N7	61.536(78)	60.010(108)	61.063(237)	60.423(164)
N3−O4−N7/\O2−O4−N3	58.857(84)	59.822(85)	58.903(209)	59.293(154)
N3−O6−N7/\N5−N7−O6	40.294(83)	42.125(109)	41.266(213)	42.101(167)
N3−O6−N7/\O2−O6−N3	61.496(88)	62.808(99)	61.939(212)	61.769(172)
O6−N7−N5/\O9−O6−N5	43.186(79)	41.482(106)	42.592(202)	42.704(185)
O6−N7−N5/\N7−N5−O7	58.251(76)	57.682(116)	57.794(208)	57.337(181)
N7−N5−O7/\O1−N5−07	69.998(91)	68.868(117)	69.231(222)	69.045(172)
N5−O1−O7/\N5−O1−O9	9.343(104)	12.077(126)	10.494(264)	11.659(181)
N5−N7−O7/\O4−O7−N7	47.639(89)	48.317(103)	48.432(194)	48.336(175)
O9−N5−O1/\O6−O9−N5	75.945(74)	76.280(88)	75.667(177)	75.534(139)
O9−N5−O1/\O2−O1−O9	48.206(97)	45.492(118)	47.242(227)	45.936(186)
O2−O9−01/\O6−O9−O2	61.635(81)	62.463(88)	62.000(171)	63.007(151)
O2−O9−O1/\O1−O4−O2	61.703(78)	63.373(101)	62.391(204)	62.505(144)
O2−O1−O4/\N3−O4−O2	36.906(80)	35.38(10)	36.460(201)	35.951(157)
O2−N3−O6/\O2−O6−O9	31.373(83)	30.220(115)	31.006(233)	30.570(182)
O2−O9−O6/\N5−O6−O9	52.905(93)	54.294(106)	53.590(197)	53.385(179)
O2−N3−O4/\O6−O2−N3	64.060(74)	63.181(90)	63.696(196)	63.984(153)
AM	0.520404	0.7604335	0	0.6186887

[a]Dihedral angles and AM values of complexes **7** and **8** (Table S1) and complexes **2** and **4** (Table S2) can be found in the Supplementary Information.

isotropic nature of the Gd^{III} ions, the decrease in the χT product can be directly correlated to antiferromagnetic interactions between the two metal centers. This interaction can be quantified by applying the van Vleck equation to Kambe's vector coupling scheme using the Hamiltonian $H = -J S_a \cdot S_b$, where $S_a = S_b = 7/2$. The best-fit parameters which reproduce the χT curve are $J = -0.02$ cm^{-1} and $g = 1.97$. The relatively weak interaction between lanthanide ions is comparable to other lanthanide systems and is due to the buried nature of the 4f orbitals, thus limiting their communication with other centers.

The field (H) dependent magnetization (M) data, plotted as M versus H and M versus H/T for all complexes are presented in the Supporting Information, Figures S10−S17. For **4**−**8**, the magnetization curves at different temperatures neither saturate in the M versus H plot nor superimpose on a single master-

dx.doi.org/10.1021/ic402682r | Inorg. Chem. XXXX, XXX, XXX−XXX

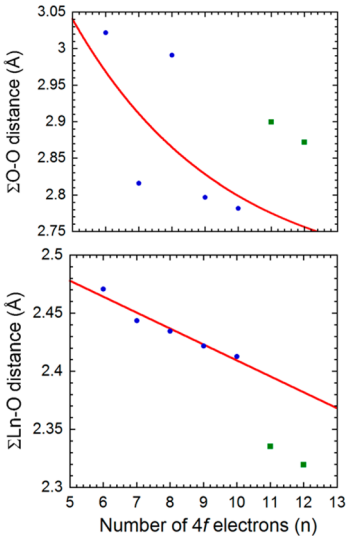

Figure 10. (top) Graph of $\Sigma_m d_{(Ln-O)}$ versus the number of 4f electrons (n) for coordinating oxygen atoms for Type I (**2**–**6**, blue) and Type II (**7** and **8**, green) analogues. Type Ia and Type Ib can clearly be distinguished in this figure. (bottom) Graph of $\Sigma_m d_{(O-O)}$ versus the number of 4f electrons (n) for oxygen atoms within the coordination polyhedra for Type I (**2**–**6**, blue) and Type II (**7** and **8**, green) analogues.

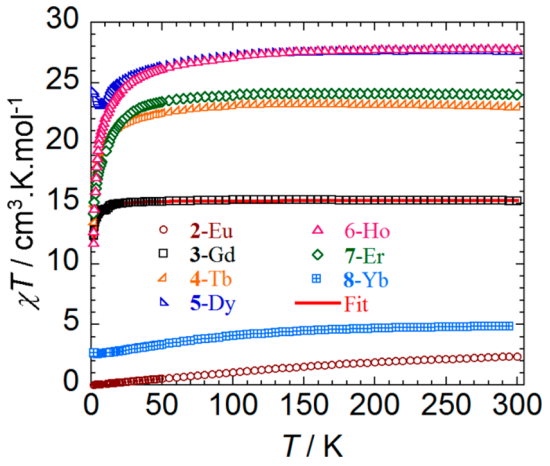

Figure 11. Temperature dependence of the χT product at 1000 Oe for complexes **2**–**8** (with $\chi = M/H$ normalized per mole). Solid red line indicates the fit.

curve in the M versus H/T plot, indicating the presence of significant magnetoanisotropy and/or the presence of low-lying excited states. For **3**, since the Gd^{III} ion is isotropic in nature, the magnetization curve at 1.8 K can be fit using a Brillouin function, which results in a g value of 1.91 for $S = 7/2$. This is in reasonable agreement with the values derived from the χT versus T fit discussed above. For **2**, the diamagnetic ground state of the Eu^{III} centers is thermally populated, resulting in a magnetization that is close to zero, as expected.

To probe potential slow magnetization relaxation, ac magnetic measurements were carried out for **5**, **7**, and **8**. All other complexes with a potential of exhibiting slow relaxation were measured as well; however, only **5**, **7**, and **8** showed a signal in the out-of-phase magnetic susceptibility (χ'') versus frequency (υ) plot. For **5**, under a zero applied dc field, significant quantum tunneling of the magnetization (QTM) was observed, preventing the occurrence of full peaks. However, by applying a field, the QTM was minimized, revealing full peaks in the χ'' versus υ plot shown in Figure 12.

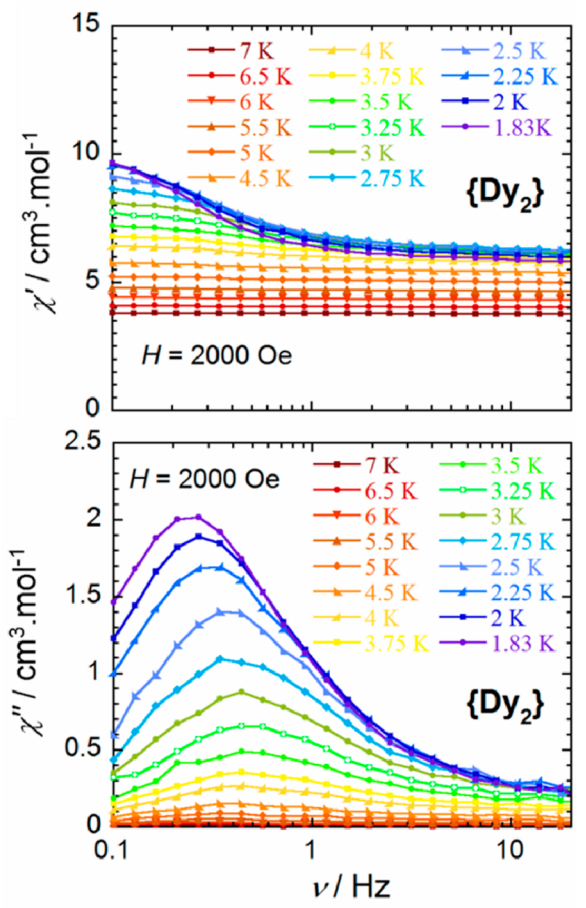

Figure 12. Frequency (υ) dependence of the (top) in-phase χ' and (bottom) out-of-phase χ'' magnetic susceptibility for **5** under an applied optimum dc field of H_{dc} = 2000 Oe.

The optimum applied dc field, where the minimum of the characteristic frequency was observed, was determined to be H_{dc} = 2000 Oe. The presence of peaks that shift to lower frequency as the temperature decreases is indicative of slow magnetization relaxation. The anisotropic energy barrier was fit using the Arrhenius equation ($\tau = \tau_0 \exp(U_{eff}/kT)$), which resulted in U_{eff} = 2.4 K (τ_0 = 0.16 s). For complex **7**, a signal was indeed observed in the χ' and χ'' versus υ plots; however, the signal-to-noise ratio was low, preventing the calculation of an energy barrier (Supporting Information, Figure S18) even when a significant amount of sample was added.

For complex **8**, the slow magnetization relaxation was also observed with a dependence on the applied dc field (Supporting Information, Figure S19). As the field was increased, two separate relaxation processes were observed under 900 and 6000 Oe. Under the former applied field (Figure 13, top) frequency-dependent peaks were evident, with an energy barrier for this relaxation process of U_{eff} = 3.1 K (τ_0 = 5.17 × 10^{-5} s). On the other hand, under 6000 Oe applied static field, a relaxation process was observed in the low-frequency region (Figure 13, bottom), with an energy barrier of U_{eff} = 3.6 K (τ_0 = 3.65 × 10^{-2} s). We believe that the multiple relaxation processes arise from the spin-flip through different

dx.doi.org/10.1021/ic402682r | Inorg. Chem. XXXX, XXX, XXX–XXX

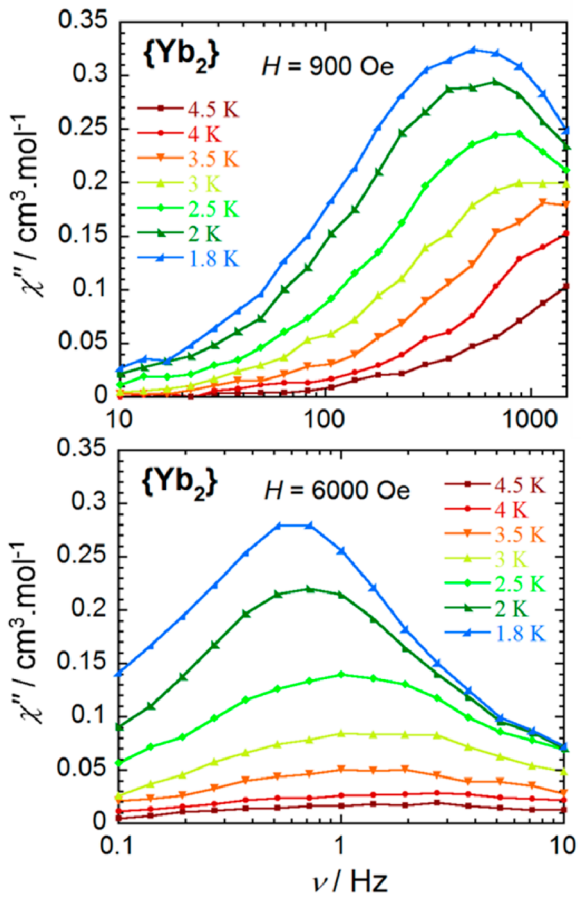

Figure 13. Frequency (υ) dependence of the out-of-phase χ'' magnetic susceptibility for complex **8** under applied dc fields of (top) H_{dc} = 900 and (bottom) 6000 Oe, revealing two relaxation processes.

excited states. Depending on the field applied, different states come into resonance, and slow relaxation of the magnetization can be observed. While a Yb complex behaving as an SMM[7] and field-dependent relaxation with multiple pathways have been observed previously, a dinuclear Yb-based SMM showing field-dependent relaxation behavior has never been previously reported.[28]

CONCLUSIONS

The effects of the lanthanide contraction on the structural and magnetic features of dinuclear complexes were investigated. As the ionic radius of the metal ions decreased with increasing number of 4f electrons, a structural rearrangement of the Type I analogues (complexes **1**−**6**) was observed, resulting in the Type II compounds (**7** and **8**). While subtle changes in the structure due to the well-known contraction in the lanthanide series have been reported previously, such a drastic change, resulting in a completely new complex, is quite rare. As the reaction conditions were identical for all complexes, this change can be attributed solely to the lanthanide contraction, with the rearrangement occurring between Ho^{III} and Er^{III}. The drastic structural rearrangement unique to this system can potentially be employed in lanthanide separation techniques, in which the dinuclear complex formed is dependent on the identity of the lanthanide ions in solution. The magnetic properties revealed a weak intramolecular antiferromagnetic interaction between Gd^{III} ions in the $\{Gd_2\}$ analogue, with $J = -0.02$ cm^{-1}, as well as slow magnetization relaxation under an applied dc field for the $\{Dy_2\}$ (**5**), $\{Er_2\}$ (**7**), and $\{Yb_2\}$ (**8**) complexes. For **8**, different slow relaxation processes were observed at different applied dc fields, rendering this complex the first dinuclear Yb-based SMM to show such field-dependent relaxation behavior.

ASSOCIATED CONTENT

Supporting Information

X-ray powder diffraction spectra for complexes **1**−**3** and **5**−**8**; structures of complexes in CIF files; additional packing diagrams for complexes **5** and **7**; additional tables of analogous measurement (AM) for complexes **7** and **8** as well as for complexes **2** and **4**; field dependence of the magnetization plots for all complexes as well as ac data for complexes **7** and **8**. This material is available free of charge via the Internet at http://pubs.acs.org.

AUTHOR INFORMATION

Corresponding Author

*E-mail: m.murugesu@uottawa.ca. Phone: 613-562-5800 ext 2733. Fax: 613-562-5170.

Author Contributions

The manuscript was written through contributions of all authors. All authors have given approval to the final version of the manuscript.

Notes

The authors declare no competing financial interest

ACKNOWLEDGMENTS

We thank the University of Ottawa, the Canada Foundation for Innovation (CFI), FFCR, and NSERC (Discovery and RTI Grants, OGS and Vanier Graduate Scholarship).

REFERENCES

(1) (a) Fossheim, S.; Kellar, K. E.; Fahlvik, A. K.; Klaveness. *J. Med. Phys.* **1997**, *15*, 193−203. (b) Cardinal, H. N.; Holdsworth, D. W.; Drangova, M.; Hobbs, B.; Fenster, A. *Med. Phys.* **1993**, *20*, 15−31.

(2) (a) Binnemans, K. *Chem. Rev.* **2009**, *109*, 4283−4374. (b) Pandya, S.; Yu, J.; Parker, D. *Dalton Trans.* **2006**, 2757−2766. (c) Hänninen, P.; Härmä, H. *Springer Ser. Fluoresc.* **2011**, *7*, 47−88. (d) Eliseeva, S. V.; Bunzli, J. C. G. *New J. Chem.* **2011**, *35*, 1165−1176. (e) Kuriki, K.; Koike, Y.; Okamoto, Y. *Chem. Rev.* **2002**, *102*, 2347−2356. (f) Haswgawa, Y.; Wada, Y.; Yanagida, S.; Kawai, H.; N. Yasuda, N.; Nagamura, T. *Appl. Phys. Lett.* **2003**, *83*, 3599−3601. (g) de Bettencourt-Dias, A. *Dalton Trans.* **2007**, *22*, 2229−2241. (h) Richards, B. S. *Sol. Energy Mater. Sol. Cells* **2006**, *90*, 1189−1207.

(3) (a) Woodruff, D.; Tuna, F.; Bodensteiner, M.; Winpenny, R.; Layfield, R. *Organometallics* **2013**, *32*, 1224−1229. (b) Benelli, C.; Gatteschi, D. *Chem. Rev.* **2002**, *102*, 2369−2388.

(4) (a) Seth, M.; Dolg, M.; Fulde, P.; Scherdtfegger, P. *J. Am. Chem. Soc.* **1995**, *24*, 6597−6598. (b) Hughes, I. D.; Däne, M.; A. Ernst, A.; Hergert, W.; Lüders, M.; Poulter, J.; Staunton, J. B.; Svane, A.; Szotek, Z.; Temmermane, W. M. *Nature* **2007**, *446*, 650−653. (c) W. Küchle, W.; Dolg, M. *J. Phys. Chem.* **1997**, *38*, 7128−7133. (d) Aguila, D.; Barrios, L. A.; Velasco, V.; Arnedo, L.; Aliaga-Alcalde, N.; Menelaou, M.; Teat, S. J.; Roubeau, O.; Luis, F.; Aromi, G. *Chem.—Eur. J.* **2013**, *19*, 5881−5891.

(5) (a) Chen, R.; Tang, W.; Jiang, W.; Zhang, Y.; Jia, D. *J. Coord. Chem.* **2013**, *66*, 650−661. (b) Zurawski, A.; Rybak, J.-C.; Meyer, L. V.; Müller-Buschbaum, K. *Z. Anorg. Allg. Chem.* **2013**, *2*, 261−267. (c) Chena, W.; Chena, Y.; Liua, W.; Leib, T.; Gaoa, O.; Kimc, D.; Suc, D.; Lib, W.; Lia, Y. *J. Coord. Chem.* **2012**, *65*, 4430−4440. (d) Gerkin, R. E.; W.J. Reppart, W. J. *Acta. Crystallogr.* **1984**, *40*, 781−786. (e) Cotton, S. A.; Franckevicius, V.; Mahon, M. F.; Ooi, L. L.; Raithby, P. R.; Teat, S. J. *Polyhedron* **2006**, *25*, 1057−1068.

dx.doi.org/10.1021/ic402682r | *Inorg. Chem.* XXXX, XXX, XXX−XXX

(6) (a) Christou, G.; Gatteschi, D.; Hendrickson, D. N.; Sessoli, R. *MRS Bull.* **2000**, *25*, 66−71. (b) Bogani, L.; Wernsdorfer, W. *Nat. Mater.* **2008**, *7*, 179. (j) Coronado, E.; Day, P. *Chem. Rev.* **2004**, *104*, 5419−5448. (c) Thomas, L.; Lionti, L.; Ballou, R.; Gatteschi, D.; Sessoli, R.; B. Barbara, B. *Nature* **1996**, *383*, 145−147. (d) Sokol, J. J.; Hae, A. G.; Long, J. R. *J. Am. Chem. Soc.* **2002**, *124*, 7656−7657. (e) Maheswaran, S.; Chastanet, G.; Teat, S. J.; Mallah, T.; R. Sessoli, R.; Wernsdorfer, W.; Winpenny, R. E. P. *Angew. Chem., Int. Ed.* **2005**, *44*, 5044−5048. (f) Zaleski, C. M.; Depperman, E. C.; Kampf, J. W.; Kirk, M. L.; Pecoraro, V. L. *Angew. Chem., Int. Ed.* **2004**, *43*, 3912−3914. (g) J. Long, J.; F. Habib, F.; Lin, P.-H.; Korobkov, I.; Enright, G.; Ungur, L.; Wernsdorfer, W.; Chibotaru, L. F.; Murugesu, M. *J. Am. Chem. Soc.* **2011**, *133*, 5319−5328. (h) Habib, F.; Lin, P.-H.; Long, J.; Korobkov, I.; Wernsdorfer, W.; Murugesu, M. *J. Am. Chem. Soc.* **2011**, *133*, 8830−8833. (i) Habib, F.; Murugesu, M. *Chem. Soc. Rev.* **2013**, *42*, 3278−3288.

(7) Pointillart, F.; Le Guennic, B.; Golhen, S.; Cador, O.; Maury, O.; Ouahab, L. *Chem. Commun.* **2013**, *49*, 615−617.

(8) (a) Yanagida, S.; Hasegawa, Y.; Murakoshi, K.; Wada, Y.; Nakashima, N.; Yamanaka, T. *Coord. Chem. Rev.* **1998**, *171*, 461−480. (b) Horrocks, W. D., Jr.; Sudnick, D. R. *J. Am. Chem. Soc.* **1979**, *101*, 334−340. (c) Pointillart, F.; Le Guennic, B.; Cauchy, T.; Golhen, S.; Cador, O.; Maury, O.; Ouahab, L. *Inorg. Chem.* **2013**, *10*, 5978−5990.

(9) Fukuda, Y.; Nakao, A.; Hayashi, K. *Dalton Trans.* **2002**, *4*, 527−533.

(10) Cucinotta, G.; Perfetti, M.; Luzon, J.; Etienne, M.; Car, P.-E.; Caneschi, A.; Calvez, G.; Bernot, K.; Sessoli, R. *Angew. Chem., Int. Ed.* **2012**, *51*, 1606−1610.

(11) (a) Paufler, P.; Kramer, U. *Wiss. Z. Tech. Univ. Dresden* **2000**, *1*, 12−15. (b) Shook, R. L.; Borovik, A. S. *Inorg. Chem.* **2010**, *8*, 3646−3660.

(12) Lin, P.-H.; Burchell, T. J.; Clérac, R.; Murugesu, M. *Angew. Chem., Int. Ed.* **2008**, *47*, 8848−8851.

(13) Lin, P.-H.; Sun, W.-B.; Yu, M.-F.; Li, G.-M.; Yan, P.-F.; Murugesu, M. *Chem. Commun.* **2011**, *47*, 10993−10995.

(14) (a) Gaoa, J.-Y.; Xiongb, X.-H.; Chena, C.-J.; Xiea, W.-P.; Rana, X.-R.; Yuea, S.-T.; Liuc, Y.-L.; Caia, Y.-P. *Inorg. Chem. Commun.* **2013**, *31*, 5−12. (b) He, Z.; Gao, E.-Q.; Wang, Z.-M.; Yan, C.-H.; Kurmoo, M. *Inorg. Chem.* **2005**, *44*, 862−874. (c) Qin, X.; Ni, X.-L.; Hu, J.-X.; Chen, K.; Zhangm, Y.-Q.; Redshaw, C.; Zhu, Q.-J.; Xue, S.-F.; Tao, Z. *CrystEngComm* **2013**, *15*, 738−744.

(15) Lin, P.-H.; Korobkov, I.; Burchell, T. J.; Murugesu, M. *Dalton Trans.* **2012**, *41*, 13649−13655.

(16) (a) Sheldrick, G. M. *SHELXTL;* Siemans Analytical X-ray Instruments Inc.: Madison, WI, 1995. (b) Sheldrick, G. M. *SHELX97 − Programs for Solving and Refining X-ray Structures*; University of Gottingen, Gottingen, Germany, 1997.

(17) (a) Costes, J.-P.; Dahan, F.; Nicodeme, F. *Inorg. Chem.* **2001**, *40*, 5285−5287. (b) Chailuecha, C.; Youngme, S.; Pakawatchai, C.; Chaichit, N.; van Albada, G.; Reedijk, J. *Inorg. Chim. Acta.* **2006**, *359*, 4168−4178. (c) Kumar, J. A.; Viswanathan, B.; Carolina, S. E. *Inorg. Chem.* **2013**, *5295*, 2432−2438. (d) Chaudhari, A. K.; Joarder, B.; Riviere, E.; Rogez, G.; Ghosh, S. K. *Inorg. Chem.* **2012**, *17*, 9159−9161.

(18) (a) Gunjan, J.; Awadh, D. *Int. Res. J. Pharm.* **2011**, *11*, 100. (b) Jadon, G.; Kumawat, L. *Int. J. Pharma Sci. Res.* **2011**, *10*, 2572−2576.

(19) Lin, S.-Y.; Xu, G.-F.; Zhao, L.; Guo, Y.; Tang, J. *Dalton Trans.* **2011**, *40*, 8213−8217.

(20) Patroniak, V.; Stefankiewicz, A.; Lehn, J.-M.; Kubicki, M.; Hoffman, M. *Eur. J. Inorg. Chem.* **2006**, *1*, 144−149.

(21) Bertini, I.; Sabatini, A. *Inorg. Chem.* **1966**, *5*, 1025−1028.

(22) (a) Bakker, J.; Deacon, G.; Forsyth, C.; Junk, P.; Wiecko, M. *Eur. J. Inorg. Chem.* **2010**, *18*, 2813−2825. (b) Zhang, S.-G.; Shi, J.-M. *Acta Crystallogr.* **2007**, *E63*, m1775−m1776.

(23) (a) Sellers, H.; Ulman, A.; Shnidman, Y.; Eilers, J. E. *J. Am. Chem. Soc.* **1993**, *115*, 9389−9401. (b) Hakkinen, H. *Nat. Chem.* **2012**, *4*, 443−455. (c) Pensa, E.; Cortes, E.; Corthey, E.; Carro, G.; Vericat, C.; Fonticelli, M. H.; Benitez, G.; Rubert, A. A.; Salvarezza, R. C. *Acc. Chem. Res.* **2012**, *45*, 1183−1192. (d) Yamashita, M. M.; Wesson, L.; Eisenman, G.; Eisenberg, D. *Proc. Natl. Acad. Sci. U.S.A.* **1990**, *87*, 5648−5652. (e) Zhu, Q.; Wegener, S. L.; Xie, C.; Uche, O.; Neurock, M.; Marks, T. J. *Nat. Chem.* **2013**, *2*, 104−109.

(24) Holmberg, R. J.; Hutchings, A.-J.; Habib, F.; Korobkov, I.; Scaiano, J. C.; Murugesu, M. *Inorg. Chem.* **2013**, *52*, 14411−14418.

(25) (a) Khoshnavazi, R.; Bahrami, L.; Gholamyan, S. *J. Mol. Struct.* **2011**, *990*, 57−62. (b) Shannon, R. D. *Acta Crystallogr.* **1976**, *A32*, 751. (c) Bünzli, J.-C. G.; Piguet, C. *Chem. Rev.* **2002**, *102*, 1897−1928.

(26) Seitz, M.; Oliver, A. G.; Raymond, K. N. *J. Am. Chem. Soc.* **2007**, *36*, 11153−11160.

(27) Ishikawa, N.; Iino, T.; Kaizu, Y. *J. Am. Chem. Soc.* **2002**, *124*, 11440−11447.

(28) (a) Rinehart, J. D.; Meihaus, K. R.; Long, J. R. *J. Am. Chem. Soc.* **2010**, *132*, 7572−7573. (b) Jeletic, M.; Lin, P.-H.; Le Roy, J. J.; Korobkov, I.; Gorelsky, S. I.; Murugesu, M. *J. Am. Chem. Soc.* **2011**, *133*, 19286−19289. (c) Car, P.-E.; Perfetti, M.; Mannini, M.; Favre, A.; Caneschi, A.; Sessoli, R. *Chem. Commun.* **2011**, *47*, 3751−3753. (d) Jiang, S.-D.; Wang, B.-W.; Sun, H.-L.; Wang, Z.-M.; Gao, S. *J. Am. Chem. Soc.* **2011**, *133*, 4730−4733.